

Stochastic Fluid Dynamics Simulations for the Velocity Distribution of Protoplasmic Streaming

Vladislav Egorov¹, Olga Maksimova¹, Irina Andreeva², Hiroshi Koibuchi^{3,*}, Satoshi Hongo³, Shinichiro Nagahiro³, Toshiyuki Ikai³, Madoka Nakayama³, Shuta Noro³, Tetsuya Uchimoto⁴, and Jean-Paul Rieu⁵

¹ Cherepovets State University (ChSU), 162600, Prospekt Lunacharskogo,

5, Cherepovets, Vologda Oblast, Russian Federation

² Peter the Great St. Petersburg Polytechnic University (SPbPU),
195251, Polytechnicheskaya, 29, St. Petersburg, Russian Federation

³ National Institute of Technology (KOSEN), Sendai College,
48 Nodayama, Medeshima-Shiote, Natori-shi, Miyagi 981-1239, Japan

⁴ Institute of Fluid Science (IFS), Tohoku University,
2-1-1 Katahira, Aoba-ku Sendai 980-0812, Japan

⁵ Univ Lyon, Université Claude Bernard Lyon 1, CNRS UMR-5306,
Institut Lumière Matière, F-69622, VILLEURBANNE, France

Protoplasmic streaming in plant cells is driven by the myosin molecule, which is called the molecular motor. The molecular motor also activates flows on/inside animal cell membranes; therefore, protoplasmic streaming has attracted considerable interest and has been extensively studied. However, the experimentally observed velocity distribution, which exhibits two peaks at $V_x = 0$ and finite $V_x (\neq 0)$ along the flow direction x , remains to be studied. In this paper, we numerically study whether the behaviour of the flow field can be simulated by a 2D stochastic Navier-Stokes (NS) equation in which Brownian random force is assumed. We present the first numerical evidence that these peaks are reproduced by the stochastic NS equation, which implies that the Brownian motion of fluid particles plays an essential role in the presence of peaks in the velocity distribution. We also discuss the dependence of the flow field on the strength D of the Brownian random force in detail.

I. INTRODUCTION

A circular flow called protoplasmic streaming is observed directly in the cells of specific plants, such as *Chara corallina* and *Nittella flexilis*, of which the cell size is relatively large ranging from a few hundred [μm] to one [mm] [1–5]. The role of streaming inside cells is naturally considered to be transportation of biological materials.

The driving force of the flow is known to be caused by a molecule moving along actin filaments; hence, it is called the molecular motor [6–11]. This molecular motor transports chlorophyll, which is very large and drives the flows in plant cells. Interestingly, the speed of the flow in cells is closely related to the size of the plant [12]. Moreover, the mechanism for transportation of biological materials is understood to be the same as that in animal cells [13, 14].

Therefore, protoplasmic streaming has attracted substantial attention both scientifically and agriculture-technologically [12]. Kamiya and Kuroda observed the position dependence of the flow speed at the section vertical to the longitudinal direction of *Nitella* cells via optical microscope in 1956 [5] (Fig. 1(a)). Later, in 1974, Mustacich and Ware observed the distribution of velocity V_x along the flow direction x by means of a laser-light scattering technique called laser Doppler velocimetry and found two different peaks at $V_x = 0$ and finite $V_x (\neq 0)$ in the velocity distribution [15, 16] (Fig. 1(b)). Measurement of the velocity distribution was performed slightly

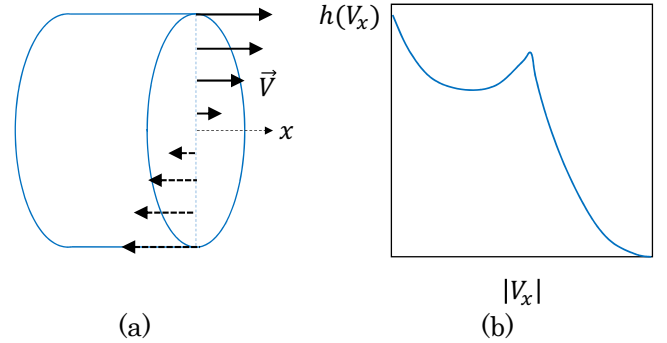


FIG. 1. (Colour online) (a) The flow velocity \vec{V} inside a cell, (b) the normalized velocity distribution $h(V_x)$ along the x -direction.

later using the same technique [17], and the two different peaks were again detected. The flow direction on the cell surface is not always parallel to the longitudinal direction but rotates around the cylindrical surface. Goldstein et al. simulated this twisting flow with the Stokes equation on a disk and reported that the velocity field is compatible with the experimental data obtained by magnetic resonance velocimetry [18–20].

However, the experimentally obtained velocity distribution is not fully understood. Although the peak at zero velocity is expected to be caused by Brownian motion of fluid molecules, as noted in Ref. [17], the peak at finite velocity is yet to be explained. Clearly, a microscopic perspective is effective for studying this problem, so we adopt Langevin simulation, which is a technique for

* koi-hiro@sendai-nct.ac.jp; koibuchih@gmail.com

simulating Brownian motion of small particles [21–26].

The peak in the velocity distribution at zero velocity is naturally understood from the fact that fluids at the central part of a cell are expected to have almost zero velocity; thus, fluid in the central region is influenced only by Brownian random forces. In contrast, fluids close to the cell wall are expected to have large velocity and be strongly influenced by the activation force of the molecular motor; in other words, thermal fluctuations are suppressed by contact with the motor and cell wall. On the other hand, fluids separated from the cell wall are not influenced by such boundary conditions, and the speed of fluids is expected decrease continuously to zero at the central region of the cell. Therefore, no intuitive explanation is available for the existence of the second peak at relatively large velocity.

In this paper, we numerically solve the Navier-Stokes (NS) equation with Brownian random force for flow fields on a square region by regarding the twisting flows as straight flow along the longitudinal direction. This two-dimensional NS equation can be considered a Langevin equation or a stochastic differential equation because it includes a random force. In this paper, we combine two different techniques [27]: NS simulation for continuum fluids [28, 29] and Langevin simulation for particles [21–26]. This simulation approach is new and, thus, is not comparable to standard techniques; therefore, we carefully check the dependence of the results on parameters including space and time discretizations. It will be shown that all qualitatively different simulation results can be obtained only by varying the strength D of the Brownian random force and that two different peaks appear in the velocity distribution at intermediate values of D .

II. STOCHASTIC NAVIER-STOKES EQUATION

A. Discretization of the Stochastic Navier-Stokes equation

As mentioned in the Introduction, the flows rotate or twist around the cell surface (Fig. 2(a)). In this paper, this twisting is neglected, and the flow direction is modified to be parallel/anti-parallel along the longitudinal direction; moreover, the original 3D flow is simplified to 2D flow (Fig. 2(b)). In this 2D model, the fluids are driven by constant velocity V_B at the boundaries.

The continuous form of the NS equation [28, 29] with Brownian random force is given by

$$\begin{aligned} \frac{\partial \omega}{\partial t} &= -(\vec{V} \cdot \nabla) \omega + \nu \Delta \omega + (\nabla \times \vec{\eta}(t))_z, \\ \omega &= -\Delta \psi, \end{aligned} \quad (1)$$

where $\vec{V} = (V_x, V_y, 0)$ is the fluid velocity obtained by stream function ψ and ω is the third component of the

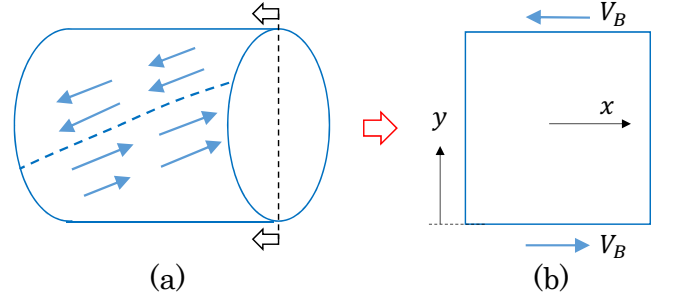


FIG. 2. (Colour online) (a) Rotating direction of the velocity on the cell surface, and (b) its simple 2D modelling for the numerical study. The velocity illustrated in (a) is not parallel to the longitudinal direction, and this skew-symmetric direction is simply modified to be parallel to the cylinder. Flows inside the surface, driven by this modified flow, are sliced at the centre for the 2D simulation model.

vorticity $\vec{\omega} = \nabla \times \vec{V}$ such that

$$\begin{aligned} V_x &= -\frac{\partial \psi}{\partial y}, \quad V_y = \frac{\partial \psi}{\partial x}, \\ \omega &= (\vec{\omega})_z, \quad \vec{\omega} = \nabla \times \vec{V}. \end{aligned} \quad (2)$$

The parameter ν in Eq. (1) is the dynamic viscosity coefficient, with $\nu \simeq 1 \times 10^{-6} [\text{m}^2/\text{s}]$ in the case of water at room temperature. The symbol $\vec{\eta}(t) = (\eta^x, \eta^y, 0)$ is Gaussian white noise or a Gaussian random force corresponding to the Brownian motion of fluid particles or a lump of fluid particles. The components of $\vec{\eta}(t)$ are assumed to satisfy

$$\langle \eta_i^\mu(t) \eta_j^\nu(t') \rangle = 2D \delta_{ij} \delta^{\mu\nu} \delta(t - t'), \quad (3)$$

where $\langle \dots \rangle$ denotes the expectation, D is called the strength of the random force and the suffix i denotes the fluid position. In Eq. (3), we introduce the discrete form of $\vec{\eta}(t)$ because the NS equation is discretized on a square lattice in the numerical study. No confusion is expected for the symbols of the dynamic viscosity ν , and the superscript of the Gaussian random force $\eta^\nu(t)$. Eq. (1) is obtained from the following NS equation

$$\rho \left[\frac{\partial \vec{V}}{\partial t} + (\vec{V} \cdot \nabla) \vec{V} \right] = -\Delta p + \mu \Delta \vec{V} + \rho \vec{\eta}(t), \quad (4)$$

where ρ and p are the density and pressure of the fluid, respectively, and $\mu = \rho \nu$ is the viscosity. This equation is conveniently modified by multiplying both sides by ρ^{-1} , and by including the condition $\nabla \cdot \vec{V} = 0$, we obtain

$$\begin{aligned} \frac{\partial \vec{V}}{\partial t} &= -(\vec{V} \cdot \nabla) \vec{V} - \rho^{-1} \Delta p + \nu \Delta \vec{V} + \vec{\eta}(t), \\ \nabla \cdot \vec{V} &= 0. \end{aligned} \quad (5)$$

Multiplying the rotation $\nabla \times$ from the left by this standard NS equation, we obtain the NS equation in Eq. (1). The NS equation in Eq. (1) instead of Eq. (5) is used because the condition $\nabla \cdot \vec{V} = 0$ is exactly satisfied in Eq.

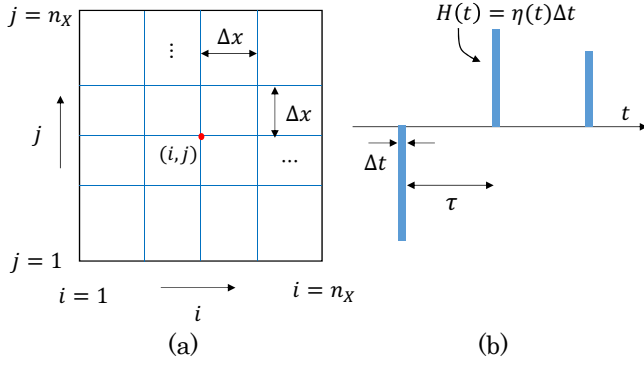


FIG. 3. (Colour online) (a) 2D regular square lattice of size $N = n_x \times n_x$, where the lattice site is denoted by (i, j) and the lattice spacing is Δx for both the i and j directions, and (b) the stochastic variable $H(t)$ proportional to Δt is understood to have a means of zero; however, its square is finite. The symbol τ in (b) corresponds to the mean time between two consecutive random forces $H(t)$, and τ should be larger than the macroscopic relaxation time τ_{re} to ensure convergence.

(1); therefore, Eq. (1) is easier to solve numerically than the original NS equation for \vec{V} in Eq. (5) in the case of protoplasmic streaming [26].

To obtain the discrete form of the NS equation in Eq. (1) on a 2D regular square lattice (Fig. 3(a)), we introduce the quantity

$$\vec{H}_{i,j}(t) = \int_t^{t+\Delta t} \vec{\eta}_{i,j}(t) dt, \quad (6)$$

where $\eta_{i,j}(t)$ denotes the random force for the fluid particle at lattice site i, j at time t (Fig. 3(b)). Note that the expression of the lattice site is changed from i to i, j such that $\vec{\eta}_i \rightarrow \vec{\eta}_{i,j}$. This $\vec{H}_{i,j}(t)$ is still considered a stochastic variable and is very small because of the small Δt . From this expression in Eq. (6) and the relation in Eq. (3), it is easy to obtain

$$\langle \vec{H}_{i,j}(t) \rangle = 0, \quad \langle H_{i,j}^2(t) \rangle = 2D\Delta t, \quad (7)$$

which are typical to stochastic variables. The first relation comes from the fact that $\vec{\eta}_{i,j}$ is Gaussian white noise with an expected value of zero, where the time integration and the mean value operation $\langle \dots \rangle$ are assumed to be commutative. If we rewrite $H_{i,j}(t)$ in Eq. (6) as

$$\vec{H}_{i,j}(t) = \vec{\eta}_{i,j}(t)\Delta t, \quad (8)$$

and insert this $H_{i,j}(t)$ into the second part of Eq. (7), we obtain a finite value

$$|\eta_{i,j}^\mu(t)| = \sqrt{2D/\Delta t} \quad (9)$$

for the Brownian random force. This expression is used for the discrete version of Eq. (1), which is given by

$$\begin{aligned} \omega_{i,j}(t + \Delta t) &\leftarrow \omega_{i,j}(t) - \Delta t \left(\vec{V} \cdot \nabla \right) \omega_{i,j}(t) \\ &+ \nu \Delta t \Delta \omega_{i,j}(t) + \sqrt{2D\Delta t} (\nabla \times \vec{g}_{i,j}(t))_z, \\ \omega_{i,j} &= -\Delta \psi_{i,j}, \end{aligned} \quad (10)$$

where $\vec{g}_{i,j}(t) = (g_{i,j}^x(t), g_{i,j}^y(t), 0)$ and the component of $\vec{g}_{i,j}$ is given by a Gaussian random number with mean 0 and variance 1. This $\vec{g}_{i,j}(t)$ is connected to $\vec{\eta}_{i,j}$ by

$$\vec{\eta}_{i,j} \Delta t = \sqrt{2D\Delta t} \vec{g}_{i,j}(t). \quad (11)$$

On the right-hand side of the first equation in Eq. (10), the spatial discretization of the second term with respect to the lattice spacing Δx is given by

$$\begin{aligned} -\Delta t \left(\vec{V} \cdot \nabla \right) \omega &= -\Delta t \left(\frac{\partial \psi}{\partial y} \frac{\partial \omega}{\partial x} - \frac{\partial \psi}{\partial x} \frac{\partial \omega}{\partial y} \right) \\ &\rightarrow -\frac{\Delta t}{4(\Delta x)^2} [(\psi_{i,j+1} - \psi_{i,j-1})(\omega_{i+1,j} - \omega_{i-1,j}) \\ &- (\psi_{i+1,j} - \psi_{i-1,j})(\omega_{i,j+1} - \omega_{i,j-1})]. \end{aligned} \quad (12)$$

This term makes almost no contribution to the flow because the velocity is low (up to $\sim 100[\mu\text{m/s}]$) in the case of protoplasmic streaming. Thus, the results are expected to be independent of whether this term is present, although the term is included in the equation for our simulations. The discrete form of Laplace operator Δ on $\omega_{i,j}$ is given by

$$\Delta \omega_{i,j} \rightarrow (1/\Delta x)^2 (\omega_{i+1,j} + \omega_{i-1,j} + \omega_{i,j+1} + \omega_{i,j-1} - 4\omega_{i,j}), \quad (13)$$

and $\Delta \psi_{i,j}$ in the second equation in Eq. (10) has almost the same discrete expression. The discrete form of the final term is given by

$$\begin{aligned} (\nabla \times \vec{g}_{i,j}(t))_z &\rightarrow \\ (g_{i+1,j}^y - g_{i-1,j}^y - g_{i,j+1}^x + g_{i,j-1}^x)/(2\Delta x). \end{aligned} \quad (14)$$

Notably, $\sqrt{2D\Delta t}$ in Eq. (10) effectively corresponds to the deviation of Brownian random force. From the dimensional analysis, $(\sqrt{2D\Delta t})^2 \Delta t = 2D(\Delta t)^2$ is the diffusion constant D_{dif} related to the temperature T by means of the Einstein-Stokes-Sutherland formula $D_{\text{dif}} = k_B T / 6\pi\mu a$, which is identified with $2D(\Delta t)^2$. Here, we introduce the notion of macroscopic relaxation time τ_e , which is the time for fluid to equilibrate from the resting state to stationary state compatible with the boundary condition given by the velocity V_B (Fig. 2(b)), and this τ_e is independent of whether the initial state is resting or random [30–33]. According to this definition, τ_e is proportional to the area (or volume in general), in sharp contrast to the standard relaxation time, which is the mean time for a molecule to return to its original position from a disturbed position. We replace Δt with τ_e because Δt is a numerically introduced quantity; thus, we have

$$2D\tau_e^2 (= D_{\text{dif}}) = \frac{k_B T}{6\pi\mu a}, \quad (15)$$

where $\mu (= \rho\nu)$ is the viscosity, a is the size of a fluid particle or lump of fluid particles in fluids, k_B is the Boltzmann constant and T is the temperature. Note that a is larger than the size of a molecule such as water because it is obtained by assuming τ_e , which is not a microscopic quantity.

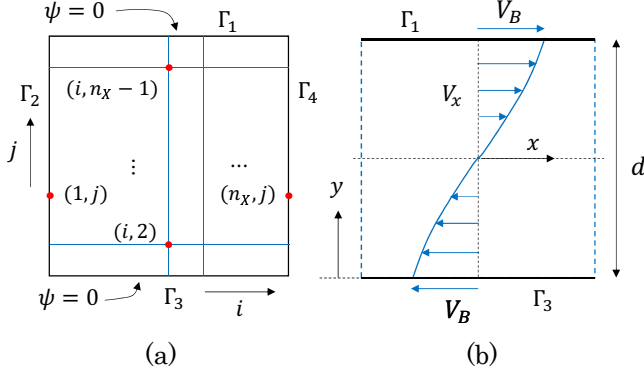


FIG. 4. (Colour online) (a) The boundary condition $\psi=0$ at the boundaries Γ_1 and Γ_3 , and (b) the velocity $\vec{V}=(V_x, V_y)$ is fixed to $\vec{V}=(V_B, 0)$ at Γ_1 and $\vec{V}=(-V_B, 0)$ at Γ_3 . The lattice sites (i, n_X-1) , $(i, 2)$ close to Γ_1 , Γ_3 in (a) are used for the boundary conditions of the variable ω in Eq. (16).

B. Boundary conditions

The boundary conditions for the variables ω and ψ at the boundaries Γ_1 and Γ_3 (Fig.4(a)) are given by

$$\begin{aligned} \omega_{i,n_X} &= -\frac{2}{(\Delta x)^2} (\psi_{i,n_X-1} + |V_B| \Delta x), \\ \psi_{i,n_X} &= 0 \quad (\text{on } \Gamma_1), \\ \omega_{i,1} &= -\frac{2}{(\Delta x)^2} (\psi_{i,2} + |V_B| \Delta x), \quad \psi_{i,1} = 0 \quad (\text{on } \Gamma_3), \end{aligned} \quad (16)$$

where the velocity \vec{V} at the boundary is given by

$$\vec{V} = (V_B, 0) \quad \text{on } \Gamma_1, \quad \vec{V} = (-V_B, 0) \quad \text{on } \Gamma_3, \quad (17)$$

where the third component is henceforth assumed to be zero and neglected for simplicity. The expression of ω in Eq. (16) on Γ_1 is obtained by Taylor expansion of ψ at Γ_1 from the second equation in Eq. (1) such that

$$\begin{aligned} \psi(x, y - \Delta y) &= \psi(x, y) - \frac{\partial \psi}{\partial y}(x, y) \Delta y + \frac{1}{2} \frac{\partial^2 \psi}{\partial y^2}(x, y) (\Delta y)^2 + \dots \quad (18) \\ &= 0 + V_B \Delta x - \frac{1}{2} \omega(x, y) (\Delta x)^2 + \dots, \quad \text{for } (x, y) \in \Gamma_1, \end{aligned}$$

where $\Delta y = \Delta x$ is assumed and $V_x = -\partial \psi / \partial y$ in Eq. (2) is used. The expression of $\omega_{i,1}$ on Γ_3 in Eq. (16) can be obtained in the same manner.

On the boundaries Γ_2 and Γ_4 , the periodic boundary condition along the horizontal or i direction is assumed such that

$$\begin{aligned} \omega_{n_X+1,j} &= \omega_{1,j}, \quad \psi_{n_X+1,j} = \psi_{1,j}, \\ \omega_{-1,j} &= \omega_{n_X,j}, \quad \psi_{-1,j} = \psi_{n_X,j}. \end{aligned} \quad (19)$$

These conditions imply that the lattice sites $(1, j)$ on Γ_2 and (n_X, j) on Γ_4 are next to each other (Fig. 4(a)).

C. Physical and simulation units

In the real process of protoplasmic streaming, length and time are measured by [m] and [s], while these values are [αm] and [βs] in the simulations with positive numbers α and β . We call [αm] and [βs] simulation units. The transformation rules from [m], [s] to [αm], [βs] are given by

$$1[\text{m}] = \alpha^{-1}[\alpha\text{m}], \quad 1[\text{s}] = \beta^{-1}[\beta\text{s}]. \quad (20)$$

The numerical results should be independent of the values of (α, β) , which will be discussed in greater detail. We consider the physical parameters

$$\begin{aligned} \nu[\text{m}^2/\text{s}], \quad V_B[\text{m/s}], \quad d[\text{m}], \quad \tau[\text{s}], \\ D[\text{m}^2/\text{s}^3], \quad \Delta x[\text{m}], \quad \Delta t[\text{s}], \end{aligned} \quad (21)$$

where the viscosity ν is explicitly included in Eq. (10). The velocity V_B is necessary in the boundary condition illustrated in Figs. 2(b) and 4(b). The third symbol d is the diameter illustrated in Fig. 4(b). The fourth symbol τ is the macroscopic relaxation time τ_e introduced in the final part of Section II A, which numerically corresponds to the length of time between two consecutive Brownian random forces acting on a fluid particle (see Fig. 3(b)). This length of time should not be less than τ_e ; otherwise, no equilibrium is obtained in the numerical simulations. The unit of D is given by $D[\text{m}^2/\text{s}^3]$, as discussed in Eq. (15). This unit can be obtained from the fact that the unit of the terms in Eq. (10) is $[1/\text{s}]$, which is easy to understand because ω has the unit $[1/\text{s}]$.

The final two parameters Δx and Δt in Eq. (21) are necessary only in the simulations; however, these parameter are connected to their indirect counterparts in real experimental phenomena. Indeed, these parameter have the following relations to the physical parameters d and τ

$$\Delta x = \frac{d}{n_X}, \quad \Delta t = \frac{\tau}{n_T}, \quad (22)$$

where n_X is the total number of lattice points on one edge of the lattice and n_T is the total number of iterations. The parameter τ is simply connected to the convergence of time evolution corresponding to a set of Brownian random forces $\{\eta_{ij}(t)\}$, and it physically corresponds to the macroscopic relaxation time, which is on the time scale typical of the phenomenon, as mentioned above. This convergence is controlled by the small parameter ε , which will be discussed later in the presentation section. Therefore, the exact information of τ or the macroscopic relaxation time τ_e is unnecessary, at least in the simulations. Indeed, if ε is sufficiently small, then the configuration randomized by Brownian forces can converge or be equilibrated correctly. In addition, if n_T (Δt) is not excessively large (small), then the simulation is not convergent; hence, Δt_0 should be fixed to $\Delta t_0 \leq \Delta t_{\text{cr}}$. This Δt_{cr} is considered the maximal time step satisfying the convergence criterion. Thus, the time-discretization

or time-evolution is subtle compared to the space discretization, which will be discussed in greater detail in the presentation section.

Here, we introduce two symbols: E for experimental parameters and S for simulation parameters such that

$$\begin{aligned} E &= (\nu, V, d), \\ S &= (\nu, V, D, \Delta x, \Delta t). \end{aligned} \quad (23)$$

The parameter D should be included in E ; however, it is unknown for the flows being studied. Therefore, D is included in S as an input for the simulations.

D. Invariance under unit changes

To discuss the invariance of the simulation results obtained by the discrete NS equation in Eq. (10) under unit changes, we use the notion of scale changes for the parameters m, s, n_X, n_T introduced in the preceding subsection. The scale changes are defined using positive numbers $\alpha, \beta, \gamma, \delta (> 0)$ such that

$$m, s, n_X, n_T \rightarrow \alpha m, \beta s, \gamma n_X, \delta n_T. \quad (24)$$

The first two $(m, s) \rightarrow (\alpha m, \beta s)$ are the unit changes of length and time, the third $n_X \rightarrow \gamma n_X$ is the change in lattice size, which corresponds to the change in lattice spacing $\Delta x \rightarrow \gamma^{-1} \Delta x$ in Eq. (22), and the final $n_T \rightarrow \delta n_T$ represents the change in time step $\Delta t \rightarrow \delta^{-1} \Delta t$ by means of Eq. (22). γ and δ for (n_X, n_T) are necessary in addition to α and β for (m, s) because the simulation results should be independent of the lattice spacing Δx and the time step Δt . For a change of Δx , for example, the scaling of n_X by α can be used because of the relation $\Delta x[m] = d/n_X[m] = \alpha^{-1} d/n_X[\alpha m] = d/(\alpha n_X)[\alpha m]$. Indeed, this relation implies that a unit change by α can be understood as a change in lattice size n_X . However, in this case, it is impossible to observe the dependence of the results on the lattice size n_X without affecting other parameters that depend on the length unit, which is why γ is necessary in addition to α .

First, we rewrite Eq. (10) by including the lattice spacing Δx explicitly such that

$$\begin{aligned} \omega_{i,j} \leftarrow \omega_{i,j} + \frac{\Delta t}{(\Delta x)^2} (\psi \cdots) (\omega \cdots) + \\ \nu \frac{\Delta t}{(\Delta x)^2} (\omega \cdots) + \frac{\sqrt{2D\Delta t}}{\Delta x} (g \cdots) [1/s], \end{aligned} \quad (25)$$

where $(\Delta x)^{-2} (\psi \cdots) (\omega \cdots)$ on the right-hand side represents the space discretization in Eq. (12) and $(\Delta x)^{-2} (\omega \cdots)$ and $(\Delta x)^{-1} (g \cdots)$ represent the discretizations of Laplacian $\Delta \omega$ and the rotation $(\nabla \times \vec{g})_z$, respectively. The symbol $[1/s]$ represents the unit of the terms, which in Eq. (25) is written with the physical units $[m]$ and $[s]$.

Under the scale changes in Eq. (24), $\Delta x (= d/n_X)[m]$ and $\Delta t (= \tau/n_T)[s]$ are replaced by $\alpha^{-1}\gamma^{-1}\Delta x[\alpha m]$ and $\beta^{-1}\delta^{-1}\Delta t[\beta s]$, and

we also have $\nu[m^2/s] = \alpha^{-2}\beta\nu[(\alpha m)^2/\beta s]$ and $D[m^2/s^3] = \alpha^{-2}\beta^3 D[(\alpha m)^2/(\beta s)^3]$. The units of ψ and ω are $\psi[m^2/s]$ and $\omega[1/s]$; therefore, we have $\psi[m^2/s] = \alpha^{-2}\beta\psi[(\alpha m)^2/\beta s]$ and $\omega[1/s] = \beta\omega[1/\beta s]$. From these expressions and Eq. (25), we obtain

$$\begin{aligned} \omega_{i,j} \leftarrow \omega_{i,j} + \gamma^2 \delta^{-1} \frac{\Delta t}{(\Delta x)^2} (\psi \cdots) (\omega \cdots) \\ + \gamma^2 \delta^{-1} \nu \frac{\Delta t}{(\Delta x)^2} (\omega \cdots) + \frac{\sqrt{2\gamma^2 \delta^{-1} D \Delta t}}{\Delta x} (g \cdots) [1/\beta s], \end{aligned} \quad (26)$$

where the common factor β is eliminated from both sides. In the case of $\gamma = 1$ and $\delta = 1$, nothing is changed except the units are changed from $[m]$, $[s]$ to $[\alpha m]$, $[\beta s]$. The problem is the case for $\gamma \neq 1$ or $\delta \neq 1$, where the factor $\sqrt{\gamma^2 \delta^{-1}}$ of the final term is different from $\gamma^2 \delta^{-1}$ of the second and third terms. However, if D changes according to $D \rightarrow \gamma^2 \delta^{-1} D$ under the scale change $(n_X, n_T) \rightarrow (\gamma n_X, \delta n_T)$, then $\gamma^2 \delta^{-1}$ becomes the common factor in these three terms on the right-hand side of Eq. (26). In this case, we have

$$\begin{aligned} \omega_{i,j} \leftarrow \omega_{i,j} + \gamma^2 \delta^{-1} \frac{\Delta t}{(\Delta x)^2} (\psi \cdots) (\omega \cdots) \\ + \gamma^2 \delta^{-1} \nu \frac{\Delta t}{(\Delta x)^2} (\omega \cdots) + \gamma^2 \delta^{-1} \frac{\sqrt{2D\Delta t}}{\Delta x} (g \cdots) [1/\beta s]; \end{aligned} \quad (27)$$

therefore, the convergent numerical solution is expected to remain unchanged. Indeed, in such a stationary or equilibrium configuration, the term $\omega_{i,j}(t + \Delta t)$ on the left-hand side is expected to be identical to the first term $\omega_{i,j}(t)$ on the right-hand side; hence, the common factor $\gamma^2 \delta^{-1}$ in the remaining terms can be dropped.

The velocity V for the boundary condition and the diameter d are included in the parameter E or S in Eq. (23), and their scaling properties under the unit change are given by $V[m/s] = \alpha^{-1}\beta V[\alpha m/\beta s]$ and $d[m] = \alpha^{-1}d[\alpha m]$. Thus, under the scale changes in Eq. (24), the right-hand side of Eq. (10) remains unchanged in the equilibrium configuration if the parameters $S = (\nu, V, D, \Delta x, \Delta t)$ scale according to

$$\begin{aligned} (\nu, V, D, \Delta x, \Delta t) \rightarrow \\ (\alpha^{-2}\beta\nu, \alpha^{-1}\beta V, \alpha^{-2}\beta^3\gamma^2\delta^{-1}D, \alpha^{-1}\gamma^{-1}\Delta x, \\ \beta^{-1}\delta^{-1}\Delta t). \end{aligned} \quad (28)$$

Next, we introduce the notion of equivalence in the simulation data. The simulation data, obtained by the solution of Eq. (10), are denoted by (ω, ψ) , while the experimental velocity data are denoted by $\text{Exp}(E)$ because the experimental data Exp are characterized by the parameters E in Eq. (23).

Definition 1

Two simulation data (ω_1, ψ_1) and (ω_2, ψ_2) are equivalent if the following conditions are satisfied:

- (i) the histogram of normalized velocity V_x distribution and
- (ii) the dependence of normalized V_x on y for (ω_1, ψ_1) are identical with those for (ω_2, ψ_2) .

Thus, we have proved the following statement:

Proposition 1

The solution (ω, ψ) of Eq. (10) remains unchanged if and only if the parameters $S = (\nu, V, D, \Delta x, \Delta t)$ scale according to Eq. (28) under the scale changes in Eq. (24).

Experimental data $\text{Exp}(E)$ can also be grouped into equivalent classes by means of the exact same definition. Indeed, two different experimental data $\text{Exp}(E_1)$ and $\text{Exp}(E_2)$ can be identified if the conditions in Definition 1 are satisfied.

The notion of equivalence can be introduced to the parameters S in Eq. (23).

Definition 2

Two sets of parameters $S_1 = (\nu_1, V_1, D_1, \Delta x_1, \Delta t_1)$ and $S_2 = (\nu_2, V_2, D_2, \Delta x_2, \Delta t_2)$ are called equivalent if there exists a set of positive numbers $\alpha, \beta, \gamma, \delta (> 0)$ such that

$$\begin{aligned} &(\nu_1, V_1, D_1, \Delta x_1, \Delta t_1) \\ &= (\alpha^{-2}\beta\nu_2, \alpha^{-1}\beta V_2, \alpha^{-2}\beta^3\gamma^2\delta^{-1}D_2, \\ &\quad \alpha^{-1}\gamma^{-1}\Delta x_2, \beta^{-1}\delta^{-1}\Delta t_2), \end{aligned} \quad (29)$$

and this equivalence is written as $S_1 \equiv S_2$. It is easy to check that $S_2 \equiv S_1$ if $S_1 \equiv S_2$ because α, β can be inverted to α^{-1}, β^{-1} . $S_1 = S_2$ if and only if $\alpha = \beta = \gamma = \delta = 1$. A set of parameters equivalent to $S = (\nu, V, D, \Delta x, \Delta t)$ is written as $\bar{S} = (\bar{\nu}, \bar{V}, \bar{D}, \bar{\Delta x}, \bar{\Delta t})$.

Notably two different parameters $S_i, (i = 1, 2)$ produce the same solution (ω, ψ) of the discrete NS Eq. (10) if $S_i, (i = 1, 2)$ are equivalent; in other words, two solutions (ω_1, ψ_1) and (ω_2, ψ_2) are equivalent if the corresponding parameters $S_i, (i = 1, 2)$ are equivalent. In this sense, the solution of Eq. (10) depends on only the equivalent class of parameters \bar{S} . If one of the parameters is changed from $\nu \rightarrow \nu_1 (\neq \nu)$ in \bar{S} , then the parameters $(\bar{\nu}_1, \bar{V}, \bar{d}, \bar{D}, \bar{\Delta x}, \bar{\Delta t})$ are not equivalent to the original one \bar{S} .

Finally, in this subsection, we introduce the symbol

$$\begin{aligned} &\text{Exp}(E) \simeq S_0 \\ &\text{for } E = (\nu, V, d), S_0 = (\nu_0, V_0, D_0, \Delta x_0, \Delta t_0), \end{aligned} \quad (30)$$

which denotes that the experimentally observed data of the velocity distribution are equivalent to the simulation data in the sense of Definition 1. The meaning of this symbol $\text{Exp}(E) \simeq S_0$ is that “experimental data $\text{Exp}(E)$ are successfully simulated with the parameters S_0 ”.

E. Unique solution of the Navier-Stokes equation

The problem that we would like to clarify is how many parameters are sufficient to simulate the real experimental data $\text{Exp}(E)$. We must consider this problem because we have many parameters $S = (\nu, V, D, \Delta x, \Delta t)$ on which the solution of Eq. (10) is dependent, even though only their equivalent classes are meaningful. One possible answer is that only the parameter D must be changed to

simulate arbitrary $\text{Exp}(E_e)$ data, and the remaining parameters can be fixed to S_0 used for simulating certain existing experimental data $\text{Exp}(E_{e,0})$, which is not always identical to $\text{Exp}(E_e)$. This process is described in more detail in the following statement.

Theorem 1

Let $E_{e,0} = (\nu_{e,0}, V_{e,0}, d_{e,0})$ be a set parameters that characterizes $\text{Exp}(E_{e,0})$, and let S_0 be a set of parameters given by $S_0 = (\nu_0, V_0, D_0, \Delta x_0, \Delta t_0)$. In this situation, if $\text{Exp}(E_{e,0}) \simeq S_0$, then for any experimental data $\text{Exp}(E_e)$, with $E_e = (\nu_e, V_e, d_e)$ and D_e , and for any given set of (n_X, n_T) , there uniquely exists D_{sim} such that $\text{Exp}(E_e) \simeq (\nu_0, V_0, D_{\text{sim}}, \Delta x_0, \Delta t_0)$.

This theorem indicates that only one parameter D_{sim} must be varied to simulate arbitrary experimental data $\text{Exp}(E_e)$. To show demonstrate this result, we first fix the parameters α and β using the parameter sets S_0 and E_e such that

$$\alpha = \frac{\nu_e}{\nu_0} \frac{V_0}{V_e}, \quad \beta = \frac{\nu_e}{\nu_0} \left(\frac{V_0}{V_e} \right)^2. \quad (31)$$

Indeed, from the expressions $\nu_e [\text{m}^2/\text{s}] = \nu_e \alpha^{-2} \beta [(\alpha \text{m})^2 / \beta \text{s}]$ and $V_e [\text{m/s}] = V_e \alpha^{-1} \beta [\alpha \text{m} / \beta \text{s}]$, we have $\nu_0 = \nu_e \alpha^{-2} \beta$ and $V_0 = V_e \alpha^{-1} \beta$, which lead to Eq. (31). Note that α and β in Eq. (31) are those for the unit change between E_e and S_0 , and these α and β are not always identical to α_0 and β_0 between $E_{e,0}$ and S_0 .

The assumption $\text{Exp}(E_{e,0}) \simeq S_0$ implies that there exist parameters $\alpha_0, \beta_0, \gamma_0$ and δ_0 for a scale change $\text{m} \rightarrow \alpha_0 \text{m}$, $\text{s} \rightarrow \beta_0 \text{s}$, $n_X \rightarrow \gamma_0 n_X$, $n_T \rightarrow \delta_0 n_T$ such that

$$\begin{aligned} &(\nu_0, V_0, D_0, \Delta x_0, \Delta t_0) \\ &= (\alpha_0^{-2} \beta_0 \nu_{e,0}, \alpha_0^{-1} \beta_0 V_{e,0}, \alpha_0^{-2} \beta_0^3 \gamma_0^2 \delta_0^{-1} D_{e,0}, \\ &\quad \alpha_0^{-1} \gamma_0^{-1} \Delta x_{e,0}, \beta_0^{-1} \delta_0^{-1} \Delta t_{e,0}). \end{aligned} \quad (32)$$

The parameter D_e is assumed to be given in addition to E_e for $\text{Exp}(E_e)$, and it is not always identical to $D_{e,0}$. The parameters Δx_e and Δt_e are defined by

$$\Delta x_e = \gamma \Delta x_0 \alpha, \quad \Delta t_e = \delta \Delta t_0 \beta, \quad (33)$$

where Δx_0 and Δt_0 are given by

$$\Delta x_0 = \frac{d_e}{\gamma n_X} \alpha^{-1} = \frac{d_e}{\gamma n_X} \frac{\nu_0}{\nu_e} \frac{V_e}{V_0} [\alpha \text{m}], \quad (34)$$

$$\Delta t_0 = \frac{\tau_e}{\delta n_T} \beta^{-1} = \frac{\tau_e}{\delta n_T} \frac{\nu_0}{\nu_e} \left(\frac{V_e}{V_0} \right)^2 [\beta \text{s}]. \quad (35)$$

The parameter γ/γ_0 is obtained from the constraint that Δx_0 in Eq. (34) in the unit $[\alpha \text{m}]$ for the simulation of $\text{Exp}(E_e)$ is identical to Δx_0 in the unit $[\alpha_0 \text{m}]$ for the simulation of $\text{Exp}(E_{e,0})$, and we have

$$\frac{\gamma}{\gamma_0} = \frac{d_e}{d_{e,0}} \frac{\nu_{e,0}}{\nu_e} \frac{V_e}{V_{e,0}}. \quad (36)$$

This expression indicates that γ is uniquely determined because the parameters involved in the expression are

already uniquely given. The uniqueness of the parameter δ is understood from the expression obtained by the same procedure such that

$$\frac{\delta}{\delta_0} = \frac{\tau_e}{\tau_{e,0}} \frac{\nu_{e,0}}{\nu_e} \left(\frac{V_e}{V_{e,0}} \right)^2, \quad (37)$$

although we must assume that the macroscopic relaxation time τ_e is a well-defined quantity in the target experiments corresponding to $E_{e,0}$ and E_e .

Using D_e , Δx_e and Δt_e , we define a set of parameters S_e such that

$$S_e = (\nu_e, V_e, D_e, \Delta x_e, \Delta t_e). \quad (38)$$

The strength D_{sim} of the random force is fixed to

$$D_{\text{sim}} = \alpha^{-2} \beta^3 \gamma^2 \delta^{-1} D_e, \quad (39)$$

which is unique because the quantities on the right-hand side are all uniquely given. Thus, we have proven that

$$\begin{aligned} &(\nu_0, V_0, D_{\text{sim}}, \Delta x_0, \Delta t_0) \\ &= (\alpha^{-2} \beta \nu_e, \alpha^{-1} \beta V_e, \alpha^{-2} \beta^3 \gamma^2 \delta^{-1} D_e, \\ &\alpha^{-1} \gamma^{-1} \Delta x_e, \beta^{-1} \delta^{-1} \Delta t_e). \end{aligned} \quad (40)$$

This relation in Eq. (40) implies $S_e \equiv (\nu_0, V_0, D_{\text{sim}}, \Delta x_0, \Delta t_0)$, which means that $\text{Exp}(E_e)$ can be simulated by $(\nu_0, V_0, D_{\text{sim}}, \Delta x_0, \Delta t_0)$ from Proposition 1, and concludes the proof of Theorem 1.

Remark 1

Rigorously speaking, the proof is insufficient because the macroscopic relaxation time τ_e is not always explicitly given in actual experimental data corresponding to E_e . Thus, the expressions in Eqs. (35) and (37) are meaningless. Therefore, this component is studied numerically in the final part of the presentation section. The problem to be numerically clarified is whether the scaling property in Eq. (40) is correct for the cases $\alpha = \beta = 1$ and $\gamma \neq 1$, $\delta \neq 1$. It is sufficient to check only the case of $\delta \neq 1$; however, the case of $\gamma \neq 1$ will also be checked. It will be shown that the scaling property is correct. Therefore, in the following discussions, we assume that Theorem 1 is correct.

Remark 2

The lattice spacing Δx_0 in S_0 used in Eq. (33) is defined using the experimental diameter $d_{e,0}[\text{m}]$ and the lattice size $n_{X0}(=\gamma_0 n_X)$, similar to Eq. (34), such that

$$\Delta x_0 = \frac{d_{e,0}}{n_{X0}} \alpha_0^{-1} = \frac{d_{e,0}}{n_{X,0}} \frac{\nu_0}{\nu_{e,0}} \frac{V_{e,0}}{V_0} [\alpha_0 \text{m}] \quad (41)$$

in the simulation unit for $\text{Exp}(E_{e,0})$. Since the diameter $d_{e,0}$ is included in Δx_0 , it is not explicitly included in S_0 and S_e . The parameter Δx_e on the right-hand side of Eq. (40) is not experimental and is simply defined by Eq. (33). The final parameter Δt_e in S_e is also defined by Eq. (33).

Remark 3

The implications of Theorem 1 should be emphasized. The meaning of the equivalence between

S_e and $(\nu_0, V_0, D_{\text{sim}}, \Delta x_0, \Delta t_0)$, expressed by $S_e \equiv (\nu_0, V_0, D_{\text{sim}}, \Delta x_0, \Delta t_0)$, is that any experimental data $\text{Exp}(E_e)$ characterized by the parameter E_e can be simulated by a single set of parameters $S_0 = (\nu_0, V_0, D_0, \Delta x_0, \Delta t_0)$ if D_0 is replaced with D_{sim} . To simulate other experimental data $\text{Exp}(E'_e)$, it is sufficient to replace D_{sim} with another D'_{sim} with $S'_e \equiv (\nu_0, V_0, D'_{\text{sim}}, \Delta x_0, \Delta t_0)$.

Remark 4

The meaning of $S_e \equiv (\nu_0, V_0, D_{\text{sim}}, \Delta x_0, \Delta t_0)$ simply implies that the simulation results with parameter S_e are identical to those with parameter $(\nu_0, V_0, D_{\text{sim}}, \Delta x_0, \Delta t_0)$; hence, it does not always imply that the real experimental data characterized by E_e are exactly the same as the simulation results with $(\nu_0, V_0, D_{\text{sim}}, \Delta x_0, \Delta t_0)$. The latter problem is related to the fundamental problem of whether the Langevin NS simulation can simulate real physical flows. In this paper, we assume it can, and this is the implication of the assumption that $\text{Exp}(E_{e,0}) \simeq S_0$. However, we emphasize that this assumption is only true because the experimentally observed peaks in the velocity distribution can be reproduced, which is the main result in this paper, as will be shown below. Another implication of the assumption $\text{Exp}(E_{e,0}) \simeq S_0$ is that the set of parameters in S_0 is already given. Using these parameters in S_0 and E_e , we obtain α and β via Eq. (31) for $\text{Exp}(E_e)$.

Remark 5

Although the dynamic viscosity ν is included in the NS equation of Eq. (10), Theorem 1 indicates that the simulation results are dependent on only D . This is understood from the original NS equation (5) for a velocity field without the pressure term, such as

$$\frac{\partial \vec{V}}{\partial t} = -(\vec{V} \cdot \nabla) \vec{V} + \nu \Delta \vec{V} + \vec{\eta}(t). \quad (42)$$

This equation contains two parameters ν and D as the second and final terms, respectively. The first term can be neglected for protoplasmic streaming; this term is independent of the following discussion, though it is included in Eq. (42). If the final term $\vec{\eta}$ is not present, it is easy to check that

$$\vec{V} = \left(\frac{2V_B}{d} y, 0 \right) \quad (43)$$

is the solution, which satisfies the boundary condition in Eq.(17) and is independent of ν . Thus, the problem is whether this solution is also expected to satisfy Eq. (42) and be independent of ν in the presence of $\vec{\eta}(t)$. Theorem 1 indirectly answers this question and shows that the results depend only on D in the presence of $\vec{\eta}$, although this does not always imply that the results are independent of ν .

III. SIMULATION RESULTS

A. Langevin simulation technique

The mean value of physical quantity Q is calculated by

$$Q = (1/n) \sum_{k=1}^n Q_k, \quad (44)$$

where Q_k is the k -th sample corresponding to the k -th convergent configuration $\{\omega, \psi\}_k$. The symbol n is the total number of samples. This configuration $\{\omega, \psi\}_k$, corresponding to a given set of Gaussian random forces $\{g\}_k$, is obtained by iterating the time step Δt and solving Poisson's equation in Eq. (10), and the suffix k ($1 \leq k \leq n$) corresponds to discrete time. Poisson's equation is solved via iteration. Thus, the sample Q_k in Eq. (44) is calculated from the convergent configuration $\{\omega, \psi\}_k$. The total number n of samples ranges in $1 \times 10^4 \leq n \leq 2 \times 10^4$ for all simulations.

The convergent configuration of the variable $\{\omega\}$ is obtained using the small number

$$\varepsilon = 1 \times 10^{-9} \quad (45)$$

for the time step of the NS equation such that

$$(1/N) \sum_{ij} \left| 1 - \frac{\omega_{ij}(t + \Delta t)}{\omega_{ij}(t)} \right| < \varepsilon, \quad (46)$$

and the same small number ε is assumed for the iteration of Poisson's equation such that

$$(1/N) \sum_{ij} \left| 1 - \frac{\psi_{ij}(t + \Delta t)}{\psi_{ij}(t)} \right| < \varepsilon, \quad (47)$$

from which the convergent configuration $\{\psi\}$ is obtained. $N (= \sum_{ij} 1 = n_X \times n_X)$ in Eqs. (46) and (47) is the total number of vertices or the lattice size, and the suffix ij denotes the lattice site.

Note that ε is connected to τ in Eq. (21). Indeed, this ε determines the total number of iterations n_T , which satisfies $n_T = \tau/\Delta t$ and, hence, depends only on τ for fixed Δt . From this result, it is clear that ε depends on τ . If ε is excessively large, the iterations of the NS equation and Poisson's equation do not converge. By contrast, if ε is excessively small, then n_T becomes very large, which leads to time-consuming simulations.

Here, we comment on the dependence of the results on the initial configuration of the variables $\{\omega, \psi\}$. On the boundaries Γ_1 and Γ_3 , the variables are fixed to assumed values according to the boundary condition. Inside the flow region, two possible initial configurations can be assumed for $\{\omega, \psi\}$: $\omega = \psi = 0$ and the convergent configuration $\{\omega, \psi\}_{k-1}$, where $\{\omega, \psi\}_0$ is $\omega = \psi = 0$. The results including n_T , which is the total number of iterations in the sense of the mean values, are independent of these initial configurations, implying that the macroscopic relaxation time τ_e is independent of such initial conditions.

B. Normalized velocity distribution

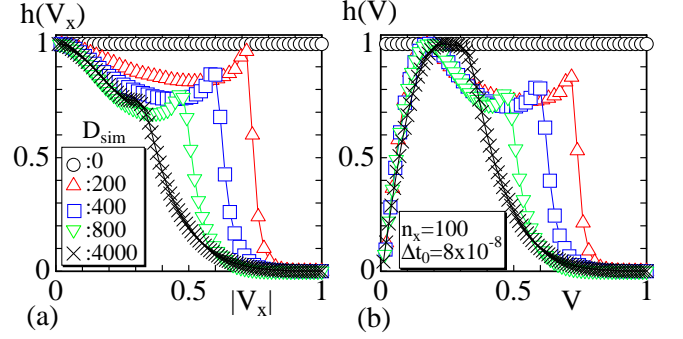


FIG. 5. (a) The distribution $h(V_x)$ of $|V_x|$ along the x -direction, and (b) the distribution of $h(V)$ of the length of \vec{V} . The lattice size is fixed to $n_X = 100$, and the strength D_{sim} of the Brownian random force is varied from $D_{\text{sim}} = 0$ to $D_{\text{sim}} = 4000$ in the simulation unit.

First, the main results are presented. In Figs. 5(a),(b), we plot the distribution or normalized histogram $h(V_x)$ of the absolute velocity $|V_x|$ along the x -direction or longitudinal direction and the distribution $h(V)$ of the magnitude V of velocity vector $\vec{V} = (V_x, V_y)$, respectively. The lattice size is fixed to $N = 10000$, where $N = n_X \times n_X$ and $n_X = 100$. According to Theorem 1, the simulation results are expected to be dependent on only the strength of Brownian random force D_{sim} ; hence, D_{sim} ranges from $D_{\text{sim}} = 0$ to $D_{\text{sim}} = 4000$ in the simulation units.

The height of the histogram $h(V_x)$ is normalized such that the maximum height is equal to 1 in each D_{sim} , and the horizontal axis $|V_x|$ is normalized using the maximum $|V_x|$ satisfying $h(V_x) \neq 0$ in each D_{sim} . The histograms $h(V)$ vs. V in Fig. 5(b) are normalized in the same way.

From Fig. 5(a), we find that $h(V_x)$ is flat for $D_{\text{sim}} = 0$ and has a peak only at $V_x = 0$ for sufficiently large D_{sim} . Another peak appears at $V_x \neq 0$ for intermediate D_{sim} . The distribution $h(V)$ in Fig. 5(b) drops to zero; $h(V) \rightarrow 0$ in the limit of $V \rightarrow 0$, in contrast to $h(V_x)$ in Fig. 5(a). This drop is reasonable because fluids are always moving and there is no fluid particle with zero velocity $\vec{V}(t) = \vec{0}$ for all t . This drop in $h(V)$ at $V \rightarrow 0$ corresponds to the fact that the same drop is visible in experimentally reported data in Ref. [15]. Indeed, in the light scattering technique, not only $\vec{V} = (V_x, 0)$ but also $\vec{V} = (V_x, V_y)$, which has a small non-zero V_y component, can be detected. The ideal gas behaviour for sufficiently large D_{sim} is also reasonable because D_{sim} is proportional to the temperature T as a result of the Einstein-Stokes-Sutherland formula; hence, for sufficiently large T , the Brownian random force is expected to be very large compared to the other interactions between fluids.

We now discuss the parameters used in the simulations in detail. The viscosity is considered to be almost 100 times larger than that of water. In Ref. [2], the viscosity

is reported to be $0.5 \leq \mu \leq 1.5[\text{dyn s/cm}^2]$. Therefore, if the density ρ is assumed to be the same as that of water, then $\nu_{e,0}$ ranges from $\nu_{e,0} = 0.5 \times 10^{-4}[\text{m}^2/\text{s}]$ to $\nu_{e,0} = 1.5 \times 10^{-4}[\text{m}^2/\text{s}]$. Thus, we assume $\nu_{e,0} = 1 \times 10^{-4}[\text{m}^2/\text{s}]$. The velocity $V_{e,0}(= 50[\mu\text{m/s}])$ at the boundary and the diameter $d_{e,0}(= 500[\mu\text{m}])$ are assumed and also shown in Table I. The parameters α_0 and β_0 in Eq. (20), which are

TABLE I. Physical parameters $E_{e,0}=(\nu_{e,0}, V_{e,0}, d_{e,0})$ in physical units assumed in the simulations, and the parameters α_0 and β_0 for the simulation units.

$\nu_{e,0}[\text{m}^2/\text{s}]$	$V_{e,0}[\mu\text{m/s}]$	$d_{e,0}[\mu\text{m}]$	α_0	β_0
1×10^{-4}	50	500	1×10^{-6}	1×10^{-1}

used in the simulations, are also shown in Table I. These values $\alpha_0 = 1 \times 10^{-6}$ and $\beta_0 = 1 \times 10^{-1}$ imply that the simulation units for length and time are $[\mu\text{m}]$ and $[0.1\text{s}]$, respectively. The first three parameters in Table I are denoted by $E_{e,0}$. These α_0 and β_0 values are obtained by Eq. (31) using the following parameters S_0 shown in Table II.

TABLE II. The parameters S_0 used in the simulations; these values are given with the simulation units. $\gamma_0 n_X$ is written as n_{X0} for simplicity.

$\nu_0[(\frac{\alpha_0 \text{m}}{\beta_0 \text{s}})^2]$	$V_0[\frac{\alpha_0 \text{m}}{\beta_0 \text{s}}]$	$\Delta x_0[\alpha_0 \text{m}]$	$\Delta t_0[\beta_0 \text{s}]$	n_{X0}
1×10^7	5	5	8×10^{-8}	100

The lattice spacing $\Delta x_0[\alpha_0 \text{m}]$ is calculated by Eq. (41). For this $\Delta x_0 = 5[\alpha_0 \text{m}]$, we have $\Delta x_{e,0} = \Delta x_0 \alpha_0^{-1} = 5 \times 10^{-6}[\text{m}]$.

There is no need to mention that the parameters S_0 in Table II are also obtained by the parameters $E_{e,0}$ in Table I and α_0 and β_0 . Indeed, it is easy to check that the viscosity $\nu_0 = 1 \times 10^7[\alpha_0^2 \text{m}^2/\beta_0 \text{s}]$ is obtained from the relation $\nu_{e,0}[\text{m}^2/\text{s}] = 1 \times 10^{-4} \beta_0/\alpha_0^2[\alpha_0^2 \text{m}^2/\beta_0 \text{s}] = \nu_0[\alpha_0^2 \text{m}^2/\beta_0 \text{s}]$. The velocity $V_0[\alpha_0 \text{m}/\beta_0 \text{s}]$ and $d_0[\alpha_0 \text{m}]$ are also obtained by the relation $V_e \alpha_0^{-1} \beta_0[\alpha_0 \text{m}/\beta_0 \text{s}] = V_0$ and $d_e \alpha_0^{-1} = d_0[\alpha_0 \text{m}]$, which is not explicitly used in the simulations.

TABLE III. The assumed parameters D_{sim} and $D_{e,0}$, the results τ_0 estimated by $\tau_0 = n_T \Delta t_0$, and the diameter a of fluid particles estimated by Eq. (15).

$D_{\text{sim}}[(\frac{\alpha_0 \text{m}}{\beta_0 \text{s}})^2]$	$D_{e,0}[\text{m}^2/\text{s}^3]$	$n_T \Delta t_0[\beta_0 \text{s}]$	$a[\text{m}]$
200	2×10^{-7}	8.7×10^{-3}	3.6×10^{-9}
400	4×10^{-7}	7.0×10^{-3}	2.8×10^{-9}
800	8×10^{-7}	7.0×10^{-3}	2.8×10^{-9}
1200	1.2×10^{-6}	1.1×10^{-2}	7.5×10^{-10}
4000	4×10^{-6}	2.6×10^{-2}	4×10^{-10}

The values of D_{sim} shown in Table III are fixed as an

input for the simulations, and the physical strength $D_{e,0}$ can be obtained by $D_{e,0} = D_{\text{sim}} \alpha_0^2 \beta_0^{-3}$. The parameter τ_0 in Table III is estimated by the relation $\tau_0 = n_T \Delta t_0$, where τ_0 is expected to satisfy $\tau_0 \geq n_T \Delta t_{\text{cr}}$, as discussed in Section II C. Using these $D_{e,0}$ and τ_0 values, we can estimate the diameter $a[\text{m}]$ of a fluid particle with Eq. (15), where the temperature is assumed to be $T=300[\text{K}]$ and $k_B T = 4.1 \times 10^{-21}[\text{Nm}]$. Although the time scale τ in Eq. (15) is expected to be smaller than τ_0 , we use the results $\tau_0 = n_T \Delta t_0$ to calculate a . This a should be larger than the size of a water molecule of $4 \times 10^{-10}[\text{m}]$, and we find that almost all data in Table III satisfy this condition. Since $n_T \Delta t_0$ is larger than the real macroscopic relaxation time, a is expected to be larger than the values in Table III if the real relaxation time is used instead of $n_T \Delta t_0$.

C. Lattice size dependence

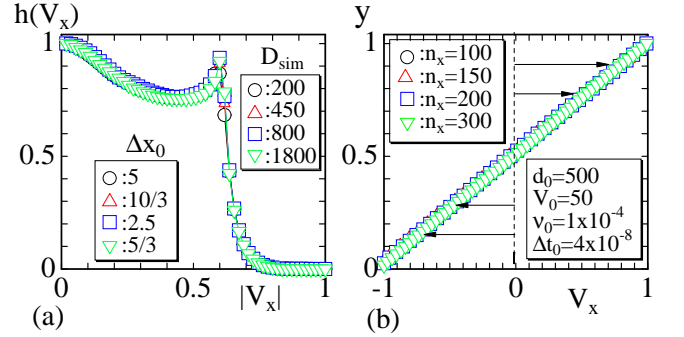


FIG. 6. (a) The distribution $h(V_x)$ obtained on lattices with size ranging from $n_X = 100$ to $n_X = 300$, and (b) the dependence of V_x on y . The parameters D_{sim} and Δx_0 are varied according to Eq. (28), and D_{sim} , Δx_0 and other parameters d_0 , V_0 , ν_0 , Δt_0 are shown in (a) and (b) in the simulation units.

In this subsection, we show that the simulation results are independent of lattice size. In Fig. 6(a), the histogram of $h(V_x)$ vs. $|V_x|$ is obtained on lattices with size ranging from $n_X = 100$ to $n_X = 300$. In those simulations, the parameters D_{sim} and Δx_0 are scaled to $\gamma^2 D_{\text{sim}}$ and $\gamma^{-1} \Delta x_0$, as indicated in Eq. (28). The results remain unchanged for a change in lattice size from $n_X (= 100)$ to γn_X , where $1 \leq \gamma \leq 3$ (see Eq. (24)). We start with $\gamma = 1$ for $D_{\text{sim}} = \gamma^2 200$ and $\Delta x_0 = \gamma^{-1} 5[\text{am}]$ with $\Delta t_0 = 4 \times 10^{-8}[\beta \text{s}]$. The parameters D_{sim} and Δt_0 can also be replaced by $D_{\text{sim}} = \gamma^2 200$ and $\Delta t_0 = 8 \times 10^{-8}[\beta \text{s}]$, which are identical to those plotted in Figs. 5(a), (b). The reason $D_{\text{sim}} = \gamma^2 400$ and $\Delta t_0 = 8 \times 10^{-8}[\beta \text{s}]$ are replaced with $D_{\text{sim}} = \gamma^2 200$ and $\Delta t_0 = 4 \times 10^{-8}[\beta \text{s}]$ is that if we start with $\Delta t_0 = 8 \times 10^{-8}[\beta \text{s}]$, the simulation does not converge for the case $\gamma = 3$.

The height of the histogram $h(V_x)$ is normalized such that the maximum height is equal to 1 in each D_{sim} , as

in Fig. 5(a), while the horizontal axes $|V_x|$ for all D_{sim} are normalized using a constant, which is the maximum $|V_x|$ of $D_{\text{sim}}=200$ of lattice $n_X=100$ satisfying $h(V_x) \neq 0$.

Additionally, the dependence of V_x on y , plotted in Fig. 6(b), is almost linear, and this linear behaviour is the same as the trivial solution in Eq. (43). Thus, the non-trivial behaviour in $h(V_x)$, which has two different peaks, is not always reflected in the dependence of V_x on y . The parameters used in the simulations are shown in Fig. 6(b).

D. Discrete time-step dependence

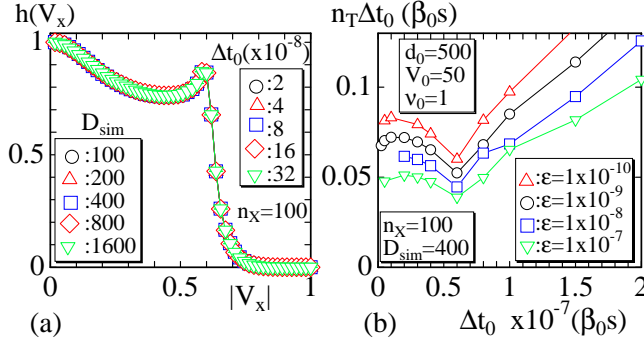


FIG. 7. (a) The distribution $h(V_x)$ vs. $|V_x|$ for different combinations of Δt_0 and D_{sim} , and (b) $n_T \Delta t_0$ vs. Δt_0 . In (a), the parameters Δt_0 and D_{sim} are varied according to $\delta^{-1} \Delta t_0$ and $\delta^{-1} D_{\text{sim}}$, where Δt_0 is changed such that $2 \times 10^{-8} \leq \Delta t_0 \leq 32 \times 10^{-8}$ in the simulation units $[\beta_0 s] = [0.1s]$.

Finally, the dependence of the results on Δt is checked. This subsection contributes to the numerical proof of Theorem 1, as indicated in Remark 1. There are two possible origins, τ and n_T , for the change in Δt , as described in Eq. (22). However, in sharp contrast to the case of diameter d for Δx , the relaxation time τ is not clear. Nevertheless, it is sufficient to see the dependence of the results on Δt or δ to check the scaling property in Eq. (28). The normalization of the histograms $h(V_x)$ vs. $|V_x|$ is defined in the same way in Fig. 6(a).

In Figs. 7(a), the histogram $h(V_x)$ of velocity vs. $|V_x|$ is plotted. The parameters D_{sim} and Δt_0 are scaled to $\delta^{-1} D_{\text{sim}}$ and $\delta^{-1} \Delta t_0$. The results are independent of Δt_0 , which is varied in the range $2 \times 10^{-8} \leq \Delta t_0 \leq 32 \times 10^{-8}$ with the simulation unit $[\beta_0 s] = [0.1s]$. This range of Δt_0 corresponds to δ ranging in $1 \leq \delta \leq 16$. Thus, the results plotted in Fig. 7(a) confirm that the scaling properties, such as $\delta^{-1} D_{\text{sim}}$ and $\delta^{-1} \Delta t_0$, are correct. This completes the numerical verification of Theorem 1.

Finally, we check whether $n_T \Delta t_0$ depends on the ε used for the convergence criteria in Eqs. (46) and (47), where ε is fixed to $\varepsilon = 1 \times 10^{-9}$ for all simulations. Here, the value is varied in $\varepsilon = 1 \times 10^{-7}$, $\varepsilon = 1 \times 10^{-8}$ and $\varepsilon = 1 \times 10^{-10}$ to assess the dependence of $n_T \Delta t_0$ on ε . The results shown

in Fig. 7(b) indicate that $n_T \Delta t_0$ are roughly independent of ε for sufficiently small Δt_0 .

E. Dependence of physical parameters

In this subsection, we demonstrate how to use Theorem 1 to discuss the dependence of the normalized velocity distribution on the physical parameters ν_e , V_e and d_e . From the perspective of Theorem 1, the simulations in Section IIIB are performed to find $S_0 = (\nu_0, V_0, D_0, \Delta x_0, \Delta t_0)$ with a suitable D_0 and the set of parameters listed in Table II. Indeed, from the simulation results, we find that $D_0 = 400$ in the second line of Table III is suitable because the shape of $h(V_x)$ in Fig. 5(a) is relatively close to the experimental data reported in Refs. [15, 16]. That is, we assume that the results with $D_0 = 400$ are similar to the reported experimental data, which play the role of $\text{Exp}(E_{e,0})$ in Theorem 1. Thus, using the parameters S_0 , we perform the simulations for $\text{Exp}(E_e)$ characterized by E_e , which is different from $E_{e,0}$.

The parameters are shown in Table IV, where ν_e , V_e , and d_e are the elements of the experimental data $E_{(i)}$, ($i = 1, 2, 3$). $E_{(1)}, E_{(2)}, E_{(3)}$ are different from $E_{e,0}$ in Table I in terms of only ν_e, V_e, d_e , respectively (denoted by underlines).

TABLE IV. The experimental data $E_{(i)}$, ($i = 1, 2, 3$), τ_e , D_e , and the corresponding parameters $\alpha, \beta, \gamma, \delta$ and D_{sim} assumed for the simulation parameters $S_{e(i)}$, ($i = 1, 2, 3$). These parameters are given by the ratio D_{sim}/D_0 , where $D_0 = 400$ from the second line of Table III.

$E_{(i)}$	$\frac{\nu_e}{\nu_{e,0}}$	$\frac{V_e}{V_{e,0}}$	$\frac{d_e}{d_{e,0}}$	$\frac{\tau_e}{\tau_{e,0}}$	$\frac{D_e}{D_{e,0}}$	$\frac{\alpha}{\alpha_0}$	$\frac{\beta}{\beta_0}$	$\frac{\gamma}{\gamma_0}$	$\frac{\delta}{\delta_0}$	$\frac{D_{\text{sim}}}{D_0}$
(1)	<u>2</u>	1	1	<u>$\frac{1}{2}$</u>	2	2	2	$\frac{1}{2}$	$\frac{1}{4}$	4
(2)	1	<u>2</u>	1	1	1	$\frac{1}{2}$	$\frac{1}{4}$	2	4	$\frac{1}{16}$
(3)	1	1	<u>2</u>	4	$\frac{1}{4}$	1	1	2	4	$\frac{1}{4}$

We assume that the macroscopic relaxation time τ_e in Eq. (15) is proportional to the inverse viscosity ν_e^{-1} [33] and the area A_e such that

$$\tau_e \sim A_e / \nu_e. \quad (48)$$

Using this relation, we obtain the ratio $\tau_e / \tau_{e,0}$ in Table IV. Consequently, from Eq. (15), we have

$$D_e \sim \frac{k_B T}{\mu a} \tau_e^{-2} \sim d_e^{-2} \nu_e, \quad (49)$$

where A_e is replaced with d_e^2 , the viscosity μ is assumed to be proportional to ν_e , and the temperature is assumed to be constant.

We now explain how to obtain the values of $\frac{D_{\text{sim}}}{D_0}$ via Theorem 1. Since $\text{Exp}(E_{e,0})$ is simulated with $S_0 =$

$(\nu_0, V_0, D_0, \Delta x_0, \Delta t_0)$, from Theorem 1, we have

$$\begin{aligned} &(\nu_0, V_0, D_0, \Delta x_0, \Delta t_0) \\ &= (\alpha_0^{-2}\beta_0\nu_{e,0}, \alpha_0^{-1}\beta_0V_{e,0}, \alpha_0^{-2}\beta_0^3\gamma_0^2\delta_0^{-1}D_{e,0}, \\ &\quad \alpha_0^{-1}\gamma_0^{-1}\Delta x_{e,0}, \beta_0^{-1}\delta_0^{-1}\Delta t_{e,0}), \end{aligned} \quad (50)$$

using the parameters $\alpha_0, \beta_0, \gamma_0, \delta_0$ for the scale change between S_0 and $S_{e,0}$. This is the assumption component or the trivial case of Theorem 1, as indicated in Remark 5, and is exactly the same as Eq. (32). We also have

$$\begin{aligned} &(\nu_0, V_0, D_{\text{sim}}, \Delta x_0, \Delta t_0) \\ &= (\alpha^{-2}\beta\nu_e, \alpha^{-1}\beta V_e, \alpha^{-2}\beta^3\gamma^2\delta^{-1}D_e \\ &\quad \alpha^{-1}\gamma^{-1}\Delta x_e, \beta^{-1}\delta^{-1}\Delta t_e), \end{aligned} \quad (51)$$

using the parameters $\alpha, \beta, \gamma, \delta$ for the scale change between S_0 and S_e . Therefore, from Table IV, we have

$$\begin{aligned} \alpha_0^{-2}\beta_0 &= 2\alpha^{-2}\beta, & \alpha_0^{-1}\beta_0 &= \alpha^{-1}\beta & \text{for } E_{(1)}, \\ \alpha_0^{-2}\beta_0 &= \alpha^{-2}\beta, & \alpha_0^{-1}\beta_0 &= 2\alpha^{-1}\beta & \text{for } E_{(2)}, \\ \alpha_0^{-2}\beta_0 &= \alpha^{-2}\beta, & \alpha_0^{-1}\beta_0 &= \alpha^{-1}\beta & \text{for } E_{(3)}, \end{aligned} \quad (52)$$

which imply

$$\begin{aligned} \alpha/\alpha_0 &= 2, & \beta/\beta_0 &= 2 & \text{for } E_{(1)}, \\ \alpha/\alpha_0 &= 1/2, & \beta/\beta_0 &= 1/4 & \text{for } E_{(2)}, \\ \alpha/\alpha_0 &= 1, & \beta/\beta_0 &= 1 & \text{for } E_{(3)}. \end{aligned} \quad (53)$$

From Eqs. (36) and (37), we have γ/γ_0 and δ/δ_0 listed in Table IV for $E_{(1)}$ and $E_{(2)}$. Thus, we obtain D_{sim}/D_0 using these values of $\alpha/\alpha_0, \beta/\beta_0, \gamma/\gamma_0, \delta/\delta_0$ and by Eqs. (50) and (51) such that

$$\frac{D_{\text{sim}}}{D_0} = \left(\frac{\alpha}{\alpha_0}\right)^{-2} \left(\frac{\beta}{\beta_0}\right)^3 \left(\frac{\gamma}{\gamma_0}\right)^2 \left(\frac{\delta}{\delta_0}\right)^{-1} \frac{D_e}{D_{e,0}}. \quad (54)$$

Therefore, the experimental data corresponding to $\text{Exp}(E_{(i)}), (i = 1, 2, 3)$ can be simulated with

$$D_{\text{sim}} = 1600 (E_{(1)}), \quad 25 (E_{(2)}), \quad 100 (E_{(3)}) \quad (55)$$

and with the parameters in Table II. Thus, we expect that the peak position of $E_{(1)}$ ($E_{(2)}$ and $E_{(3)}$) to move to the left (right) of the peak position of $E_{e,0}$. Moreover, the simulation results for $\text{Exp}(E_{(i)}), (i = 1, 2, 3)$ are located between, or are slightly different from, the curves in Figs. 5(a),(b). This is why we call the results in Section IIIB the main results, which is what we emphasize in this subsection.

IV. SUMMARY AND CONCLUSION

In this paper, we study the flow field of protoplasmic streaming in plant cells such as *Chara corallina* and *Nittella flexilis* by means of the stochastic or Langevin Navier-Stokes (NS) equation, which is a 2D equation for incompressible viscous flows with Brownian random

forces. The study is focused on the experimentally observed distribution of velocity along the flow direction, where the velocity distribution has two different peaks. We numerically find that the peaks are reproduced by the Langevin NS simulation.

The results in this paper indicate that the second peak in the large velocity region is independent of plasmagel and plasmasol between the cell wall and vacuole because such a fine structure in plant cells is neglected in the 2D simulation model. Moreover, the fact that the peaks are reproduced by the 2D model implies that the 3D nature of the real protoplasmic streaming is not essential to the existence of the second peak, although the shapes of the peaks are expected to be influenced by the dimensions.

Theorem 1, which is supported by the simulation results, implies that the effects of viscosity in real flows are reflected in the strength of Brownian random force D ; therefore, real flows can be simulated simply by changing D . This result is reasonable because the strength D is related to the diffusion constant D_{dif} in Eq. (15), where D_{dif} depends on not only temperature but also viscosity. We emphasize that fluid flow can naturally be understood in terms of such a profound relation between macroscopic and microscopic phenomena simply because of the stochastic NS equation.

As noted in the final part of Section IIIB, the dependence of V_x on y is almost linear and is slightly different from the experimentally reported result. One reason for this deviation is that the simulation model in this paper is simplified in many aspects compared with real flows. In fact, the simulation model is a 2D model and the twist of the flows and the interactions of fluids with biological materials are neglected. These neglected components should be included in the model for further fluid mechanical studies on protoplasmic streaming.

ACKNOWLEDGMENTS

The author H.K. acknowledges Kazuhiko Mitsuhashi for reminding him of this interesting field. This work is supported in part by the Collaborative Research Project of the Institute of Fluid Science (IFS), Tohoku University, and it is also supported in part by the Collaborative Research Project of the National Institute of Technology (KOSEN), Sendai College. H.K. acknowledges Prof. Jean-Yves Cavaille of INSA Lyon for the support of the IFS project and encouragement. The author V.E. acknowledges president Dr. Hiroshi Fukumura of Sendai KOSEN for the warm hospitality during a four month stay from 2019 to 2020, and this stay was supported in part by JSPS KAKENHI Grant No. JP17K05149.

REFERENCES

- [1] N. Kamiya, Cytoplasmic streaming in giant algal cells: A historical survey of experimental approaches, <https://doi.org/10.1007/BF02488723>, *Bot. Mag. Tokyo*, **99**, 441-496 (1986).
- [2] N. Kamiya and K. Kuroda, Dynamics of Cytoplasmic Streaming in a Plant Cell, *Biorheology*, **10**, 179-187 (1973).
- [3] M. Tazawa, Motive force of the cytoplasmic streaming in *Nitella*, *Protoplasma*, **65**, 207-222 (1968).
- [4] N. Kamiya and K. Kuroda, Measurement of the Motive Force of the Protoplasmic Rotation in *Nitella*, *Protoplasma*, **50**, 144-147 (1958).
- [5] N. Kamiya and K. Kuroda, Velocity Distribution of the Protoplasmic Streaming in *Nitella* Cells, <https://doi.org/10.15281/jplantres1887.69.544>, *Bot. Mag. Tokyo*, **69**, 544-554 (1956).
- [6] D. Houtman, I. Pagonabarraga, C.P. Lowe, A. Esseling-Ozdoba, A.M.C. Emons and E. Eiserle, Hydrodynamic flow caused by active transport along cytoskeletal elements, <https://doi.org/10.1209/0295-5075/78/18001>, *Europhysics Lett.* **78**, 18001(1-5) (2007).
- [7] S. Klumpp, T.M. Nieuwenhuizen, and R. Lipowsky, Movements of molecular motors: Ratchets, random walks and traffic phenomena, <https://doi.org/10.1016/j.physe.2005.05.037>, *Physica E* **29**, 380-389 (2005).
- [8] R. Lipowsky, Y. Chai, S. Klumpp, S. Liepelt, M.J.I. Müller, Molecular motor traffic: From biological nanomachines to macroscopic transport, <https://doi.org/10.1016/j.physa.2006.05.019>, *Physica A* **372**, 34-51 (2006).
- [9] T. Kawakubo, T. Kobayashi, S. Sakamoto, Drift motion of granules in chara cells induced by random impulses due to the myosin-actin interaction, *Physica A* **248** 21-27 (1998).
- [10] F. Jülicher, A. Ajdari, and J. Prost, Modeling molecular motors, *Rev. Mod. Phys.* **69**, No. 4, 1269-1281 (1997).
- [11] R.D. Astumian, Thermodynamics and Kinetics of a Brownian Motor, <https://DOI:10.1126/science.276.5314.917> *Science*. **276** (5314), 9217-922 (1997).
- [12] M. Tominaga, A. Kimura, E. Yokota, T. Haraguchi, T. Shimmen, K. Yamamoto, A. Nakano, and K. Ito, Cytoplasmic Streaming Velocity as a Plant Size Determinant, <http://dx.doi.org/10.1016/j.devcel.2013.10.005>, *Developmental Cell*, **27**, 345-352, (2013).
- [13] B.B. McIntosh and E.M. Ostap, Myosin-I molecular motors at a glance, <https://doi.org/10.1242/jcs.186403>, *J. Cell Sci.* **129**, 2689-2695 (2016).
- [14] M. Tominaga and K. Ito, The molecular mechanism and physiological role of cytoplasmic streaming, <http://dx.doi.org/10.1016/j.pbi.2015.06.017>, *Current Opinion in Plant Biology*, **27**, 104-110 (2015).
- [15] R.V. Mustacich and B.R. Ware, Observation of Protoplasmic Streaming by Laser-Light Scattering, *Phys. Rev. Lett.* **33**, 617-620 (1974).
- [16] R.V. Mustacich and B. R. Ware, Velocity Distributions of the Streaming Protoplasm in *Nitella Flexilis*, *Biophys. J.* **17**, 229-241 (1977).
- [17] D.B. Sattelle, and P.B. Buchan, Cytoplasmic Streaming in *Chara Corallina* studied by Laser Light Scattering, *J. Cell. Sci.* **22**, 633-643 (1976).
- [18] J-W. Meent, I. Tuval, and R.E. Goldstein, Nature's Microfluidic Transporter: Rotational Cytoplasmic Streaming at High Péclet Numbers, *Phys. Rev. Lett.* **101**, 178102(1-4) (2008).
- [19] R.E. Goldstein, I. Tuval and J-W. van de Meent, Microfluidics of cytoplasmic streaming and its implications for intracellular transport, <https://www.pnas.org/cgi/doi/10.1073/pnas.0707223105>, *PNAS*, **105**, 3663-3667 (2008).
- [20] R.E. Goldstein and J-W. van de Meent, Physical perspective on cytoplasmic streaming, <https://doi.org/10.1098/rsfs.2015.0030>, *Interface Focus*. **5**: 20150030.
- [21] D.S. Lemons and A. Gythiel, Paul Langevin's 1908 paper "On the Theory of Brownian Motion", *Am. J. Phys.* **65** (11), pp.1079-1081 (1997).
- [22] W. Brenig, *Statistical Theory of Heat*, Springer-Verlag Berlin Heidelberg 1989. <https://doi.org/10.1007/978-3-642-74685-7>
- [23] R. Metzler, J. Klafter, The random walk's guide to anomalous diffusion: a fractional dynamics approach, *Phys. Rep.* **339**, 1-77 (2000).
- [24] G. G. Batrouni, G. R. Katz, A. S. Kronfeld, G. P. Lepage, B. Svetitsky, and K. G. Wilson, Langevin simulations of lattice field theories, *Phys. Rev. D* **32** 2736-2747 (1985).
- [25] A. Ukawa and M. Fukugita, Langevin Simulation Including Dynamical Quark Loops, *Phys. Rev. Lett.* **55**, 1854-1857 (1985).
- [26] K. Höfler and S. Schwarzer, Navier-Stokes simulation with constraint forces: Finite-difference method for particle-laden flows and complex geometries, *Phys. Rev. E*. **61**, 7146-7160 (2000).
- [27] B. Uma, T.N. Swaminathan, R. Radhakrishnan, D.M. Eckmann, and P.S. Ayyaswamy, Nanoparticle Brownian motion and hydrodynamic interactions in the presence of flow fields, *Physics of Fluids* **23**, 073602 (2011); <https://doi.org/10.1063/1.3611026>
- [28] M.E. Taylor, *Partial Differential Equations III, Nonlinear Equations*, 2nd Edition, (New York, Springer, 2010), Chapter 17, 511-614.
- [29] G. Lukaszewicz and P. Kalita, *Navier-Stokes Equations, An Introduction with Applications*, (Springer, 2015).
- [30] W.T. Coffey and Yu.P. Kalmykov, On the calculation of the macroscopic relaxation time from the Langevin equation for a dipole in a cavity in a dielectric medium, *Chemical Physics* **169**, pp.165-172 (1993); [https://doi.org/10.1016/0301-0104\(93\)80074-J](https://doi.org/10.1016/0301-0104(93)80074-J)
- [31] Y. Feldman, A. Puenko, and Y. Ryabov, Dielectric Relaxation Phenomena in Complex Materials, in *Fractals, Diffusion, and Relaxation in Disordered Complex Systems*, Eds. W.T. Coffey and Y.P. Kalmykov, *Advanced Chemical Physics Vol.133*, Wiley-Interscience, New Jersey, 2006.
- [32] V.I. Arkhipov, Hierarchy of dielectric relaxation times in water, [https://doi.org/10.1016/S0022-3093\(02\)01089-X](https://doi.org/10.1016/S0022-3093(02)01089-X), *J. Non-Cryst. Sol.* **305**, pp.127-135 (2002)
- [33] L.I. Zaichik, V.A. Pershukov, M.V. Kozolev and A.A. Vinberg, Modeling of Dynamics, Heat Transfer, and Combustion in Two-Phase Turbulent Flows: 1. Isothermal Flows, *Exp. Therm. Fl. Sci.* **15** pp.291-310 (1997).